Graph Neural Networks for Joint Communication and Sensing Optimization in Vehicular Networks

Xuefei Li, *Graduate Student Member, IEEE*, Mingzhe Chen, *Member, IEEE*, Yuchen Liu, *Member, IEEE*, Zhilong Zhang, *Member, IEEE*, Danpu Liu, *Senior Member, IEEE*, and Shiwen Mao, *Fellow, IEEE*

***Abstract*— In this paper, the problem of joint communication and sensing is studied in the context of terahertz (THz) vehicular networks. In the studied model, a set of service provider vehicles (SPVs) provide either communication service or sensing service to target vehicles, where it is essential to determine 1) the service mode (i.e., providing either communication or sensing service) for each SPV and 2) the subset of target vehicles that each SPV will serve. The problem is formulated as an optimization problem aiming to maximize the sum of the data rates of the communication target vehicles, while satisfying the sensing service requirements of the sensing target vehicles, by determining the service mode and the target vehicle association for each SPV. To solve this problem, a graph neural network (GNN) based algorithm with a heterogeneous graph representation is proposed. The proposed algorithm enables the central controller to extract each vehicle's graph information related to its location, connection, and communication interference. Using this extracted graph information, a joint service mode selection and target vehicle association strategy is then determined to adapt to the dynamic vehicle topology with various vehicle types (e.g., target vehicles and service provider vehicles). Simulation results show that the proposed GNN-based scheme can achieve 93.66% of the sum rate achieved by the optimal solution, and yield up to 3.16% and 31.86% improvements in sum rate, respectively, over a homogeneous GNN-based algorithm and a conventional optimization algorithm without using GNNs.**

***Index Terms*— Joint communication and sensing, terahertz, vehicular networks, graph neural networks.**

I. Introduction

INTEGRATION of wireless communication and sensing functionalities on smart vehicles has been regarded as a promising paradigm to improve the safety and efficiency of vehicular networks. The joint design of communication and sensing functionalities can mutually enhance each other by leveraging the unified hardware, spectrum resource, and protocol design [2], [3], [4]. However, the scarce bandwidth of sub-6 GHz bands limits the ability of wireless networks to meet the stringent quality-of-service (QoS) requirements of emerging vehicular applications in terms of delivering high data rates and high-resolution sensing [5], [6], [7], [8], [9]. A promising solution is to use the high-frequency terahertz (THz) bands for its abundant bandwidth. However, deploying THz for joint communication and sensing over vehicular networks faces several challenges, such as severe path loss and extremely directional nature of vehicular links, interference among communication and sensing links, determining which vehicles to provide communication or sensing service, various QoS requirements of communication and sensing, and adaptation to dynamics of vehicle network topology.

A. Related Work

Recently, several works, such as [10], [11], [12], [13], [14], [15], [16], and [17], have studied the problem of resource management for joint communication and sensing. The authors in [10] and [11] provided a comprehensive survey of joint communication and sensing systems, and introduced various challenges, problems, and solutions to improve the performance of such systems. The authors in [12] studied the use of the time-domain duplex (TDD) scheme to achieve the fusion of communication and sensing. In [13], the authors optimized the scheduling of communication and sensing signals over different time slots. A time division duplex frame was proposed in [14] and [15] to determine the communication and sensing mode in each time slot. An adaptive service mode selection algorithm was designed in [16] to maximize the resource efficiency by selecting the communication and sensing modes based on service requirements. However, the existing works in [12], [13], [14], [15], and [16] might introduce mutual interference between communication and sensing systems due to inconsistent operation modes of different vehicles. To address this challenge, in [17], the authors analyzed the interference between communication and sensing services so as to optimize the time slot allocation for providing both services to each vehicle. However, these works [12], [13], [14], [15], [16], [17] did not consider the use of THz bands to provide high-rate communication and high-resolution sensing services. Using

Manuscript received 15 February 2023; revised 27 June 2023; accepted 13 August 2023. Date of publication 9 October 2023; date of current version 22 November 2023. This work was supported in part by the National Natural Science Foundation of China under Grant 61971069, Grant 62271065, and Grant U22B2001; and in part by the Beijing Natural Science Foundation under Grant L202003. An earlier version of this work [1] was presented at the Proceedings of the 2023 IEEE International Conference on Communications (ICC). *(Corresponding author: Zhilong Zhang.)*

Xuefei Li, Zhilong Zhang, and Danpu Liu are with the Beijing Laboratory of Advanced Information Network, Beijing University of Posts and Telecommunications, Beijing 100876, China (e-mail: 2013213202@bupt.edu.cn; zhangzhilong@bupt.edu.cn; dpliu@bupt.edu.cn).

Mingzhe Chen is with the Department of Electrical and Computer Engineering and the Institute for Data Science and Computing, University of Miami, Coral Gables, FL 33146 USA (e-mail: mingzhe.chen@miami.edu).

Yuchen Liu is with the Department of Computer Science, North Carolina State University, Raleigh, NC 27695 USA (e-mail: yuchen.liu@ncsu.edu).

Shiwen Mao is with the Department of Electrical and Computer Engineering, Auburn University, Auburn, AL 36849 USA (e-mail: smao@ieee.org).

Color versions of one or more figures in this article are available at https://doi.org/10.1109/JSAC.2023.3322761.

Digital Object Identifier 10.1109/JSAC.2023.3322761

THz bands can significantly improve both the data rate and sensing resolution, which however, also faces the challenges of higher path loss and attenuation [18].

To overcome such limitations, a number of existing works such as [19], [20], [21], [22], [23], [24], and [25] studied the use of the THz bands to provide communication service for mobile users. The authors in [19] investigated a target vehicle association scheme for ultra-dense THz networks while considering the THz channel particularities, the antenna directivity of the base station (BS) and users, as well as their positions and communication service requirements. The authors in [20] studied the beam alignment problem in THz communications by considering the effect of narrow beamwidth and fast mobility of connected autonomous vehicles. In [21], the authors analyzed target vehicle association schemes and multi-connectivity strategies for joint THz/millimeter wave (mmWave) deployments. The authors in [22] optimized spectrum resource allocation for downlink and uplink communications in unmanned aerial vehicle (UAV) assisted THz systems. However, all the above works [19], [20], [21], [22] simply assumed a constant THz directional antenna gain while ignoring how the main and side lobes affect THz communications. In [23], the authors studied the use of a THz band for communications and modeled the THz antenna gain as a function of beamwidth. However, this work does not consider the radiation of the side lobes of THz antennas. Although the authors in [24] and [25] studied the directional THz antenna gain of the main lobe and side lobes simultaneously, they did not consider the use of the THz bands to provide sensing service. Therefore, these existing solutions [19], [20], [21], [22], [23], [24], [25] cannot be directly applied for vehicle networks that use THz for joint communication and sensing since these two services will interfere each other. Consequently, given the high uncertainty of THz channels, it is critical to manage the vehicle topological information to avoid potential mutual interference when THz bands are used for joint communication and sensing in vehicular networks.

To manage the vehicle topological information, a number of existing works such as [26], [27], [28], [29], [30], [31], [32], and [33] studied the use of graph neural network (GNN) to extract vehicle topological information. In [26], a graph convolutional network (GCN) with weighted adjacency matrix was used to capture the spatial features of vehicle topology and describe the intensities of mutual influence between vehicles. The work in [27] trained a GCN to learn the topology related features (e.g., vehicle location, vehicle connection, and communication interference) for each user and then solved a link scheduling problem based on the extracted feature vectors. The authors in [28] used a topological GCN followed by a sequence-to-sequence framework to predict future traffic flow and density. The authors in [29] used a directed GCN to predict the motion trajectories of moving vehicles in complex traffic scenes. However, the above works [26], [27], [28], [29] required the information of all vehicles to extract the topology related feature vector for each vehicle, which may not be applied for networks with a dynamic vehicle topology. To make it adaptive to dynamic vehicle topologies, our work herein learns a node representation method with the partial vehicle topological information. The authors in [30] and [31] proposed to generate topology related feature vectors by sampling and aggregating the information from local neighbors. In [32], the authors explored the graph representation methods for link scheduling in device-to-device (D2D) networks, where D2D devices are considered as nodes and the interference among these devices are considered as edges. The authors in [33] selected a fixed number of neighborhood vehicles to participate in training to ensure that the input size will not change with the number of vehicles. However, these works [30], [31], [32], [33] only used homogeneous graphs composed of a single type of nodes and edges to represent network devices and their communication links. Hence, all the aforementioned works [26], [27], [28], [29], [30], [31], [32], [33] are not suited for extracting topology related feature vectors for joint communication and sensing enabled vehicular networks, since such networks consist of different types of vehicles (e.g., target vehicles and service provider vehicles) and connected links.

B. Contributions

The main contribution of this work is to design a novel framework that enables service provider vehicles (SPVs) to provide joint communication and sensing services to target vehicles using THz bands. *To the best of our knowledge, this is the first work to study the use of THz for joint communication and sensing in vehicular networks.* Our key contributions include:

- We consider the problem of joint communication and sensing over THz vehicular networks. In the studied model, a set of SPVs provide either communication service or sensing service to communication target vehicles or sensing target vehicles, respectively. A central controller determines the service mode (i.e., providing communication or sensing service) for each SPV and the subset of target vehicles that each SPV will serve.
- We formulate an optimization problem aiming to maximize the sum of the data rates of all communication target vehicles while satisfying the sensing service requirements of sensing target vehicles by jointly determining the service mode (i.e, communication or sensing) and the target vehicle association for each SPV. The THz channel particularities, the directivity of vehicle antennas, as well as the dynamic vehicle topological information and the sensing service requirements are all taken into account in the formulation.
- To solve the formulated problem, we propose a novel GNN method that combines GNNs with heterogeneous graphs. The proposed algorithm enables the central controller to extract each vehicle's graph information that represents the information related to vehicle location, vehicle connection, and vehicle communication interference. Compared with traditional GNN methods [30], which used a homogeneous graph to represent various types of vehicles, the proposed algorithm adopts a heterogeneous graph with various types of nodes and edges to represent different types of vehicles and their

connected links. Using the learned graph information, the probability distribution of each SPV serving each target vehicle in the corresponding operating mode is obtained. Based on the probability distribution, the non-convex optimization problem can be simplified to a quadratically constrained programming (QCP) problem, which can be solved by the Gurobi tool [34].

- Extensive simulation results show that the number of service provider vehicles, number of target vehicles, vehicle orientation, and dimension of the graph information vector will jointly affect the performance of service mode selection and target vehicle association strategy in THz enabled vehicular networks. In particular, the proposed GNN-based scheme can reach 93.66% of the sum rate produced by the optimal solution, and yield up to 3.16% and 31.86% improvement in the sum rate over a homogeneous graph neural network based algorithm and the conventional optimization algorithm without using GNNs, respectively.

The remainder of this paper is organized as follows. The system model and the problem formulation are described in Section II. The design of the GNN-based algorithm for service mode selection and target vehicle association is introduced in Section III. In Section IV, numerical results are presented and discussed. Finally, conclusions are drawn in Section IV.

II. System Model and Problem Formulation

A. Network Model

We consider a vehicular network in which a set of vehicles moving in a region, as shown in Fig. 1. The vehicles are divided into three categories: service provider vehicles $\mathcal{K}$, communication target vehicles $\mathcal{M}$, and sensing target vehicles $\mathcal{N}$. Each service provider vehicle (SPV) is equipped with both communication and sensing devices, thus can operate in either the communication mode or the sensing mode. When operating in the communication mode, an SPV communicates with the target vehicles through vehicle-to-vehicle (V2V) links. In contrast, an SPV that operates in the sensing mode can sense the location, speed, and direction of the target vehicles for further use (e.g., generate a high-definition map (HD Map)) [35]. In our model, the locations and density of vehicles vary over time with unknown distributions, and all SPVs use the same THz band to provide communication or sensing services. Here, we consider spectrum reuse to improve spectrum efficiency since THz signals suffer severe path loss. In fact, our designed method can also be used for the scenarios where orthogonal bands are allocated to each SPV and target vehicle. The main notations used in this paper are summarized in Table I.

1) THz Propagation and Antenna Model: We assume that directional three-dimensional (3D) beams are utilized at the vehicles to compensate for the severe path loss in THz bands. The antenna gains of the main lobe and the side lobes from vehicle k to vehicle m are expressed as [24]

$$G_{km}^{\mathrm{M}} = \frac{4\pi}{(\varepsilon+1)\Omega_{\theta_k,\varphi_k}}, \tag{1}$$

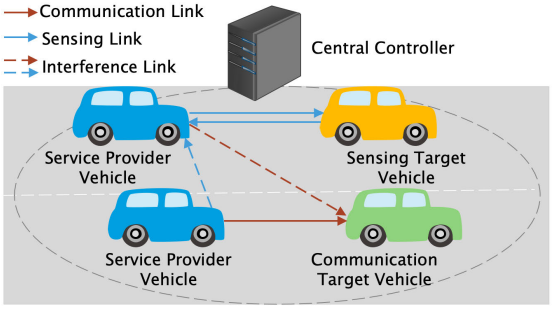

Fig. 1. Illustration of the vehicular network model.

$$G_{km}^{\mathrm{S}} = \frac{4\pi\varepsilon}{(\varepsilon+1)\left(4\pi-\Omega_{\theta_k,\varphi_k}\right)}, \tag{2}$$

where $\Omega_{\theta_k,\varphi_k} = 4\arcsin\left(\tan\left(\frac{\theta_k}{2}\right)\tan\left(\frac{\varphi_k}{2}\right)\right)$ with θ_k and φ_k being the horizontal and vertical beamwidths of the antenna for vehicle k, and ε is the ratio of the power concentrated along the side lobes to the power concentrated along the main lobe.

Signal propagation in the THz bands is determined by the molecular absorption loss and the spreading loss. The absorption loss is given by [23]

$$L_{km}^{\mathrm{A}} = \frac{1}{\tau(d_{km})}, \tag{3}$$

where d_{km} is the distance between vehicle k and vehicle m, and $\tau(d_{km}) \approx e^{-\phi(f)d_{km}}$ is the transmittance of the medium following the Beer-Lambert law with $\phi(f)$ being the overall absorption coefficient of the medium, and f is the operating frequency. Assuming free space propagation, the spreading loss is defined as

$$L_{km}^{\mathrm{F}} = \frac{(4\pi f d_{km})^2}{c^2}, \tag{4}$$

where c is the speed of light.

Therefore, the received power at vehicle m from vehicle k can be expressed as

$$S_{km} = \frac{P_k G_{km}^{\mathrm{T}} G_{mk}^{\mathrm{R}}}{L_{km}^{\mathrm{A}} L_{km}^{\mathrm{F}}}, \tag{5}$$

where P_k is the transmit power of vehicle k. G_{km}^{T} and G_{mk}^{R} are the effective antenna gains at vehicle k and vehicle m, respectively, corresponding to the link between vehicle k and vehicle m with $\mathrm{T} \in \{\mathrm{M}, \mathrm{S}\}$ and $\mathrm{R} \in \{\mathrm{M}, \mathrm{S}\}$, where M stands for the main lobe and S stands for the side lobes.

2) Communication Mode: The interference to the communication target vehicle m served by SPV k is

$$I_{km}^{\mathrm{C}}(\boldsymbol{\alpha},\boldsymbol{\beta}) = \sum_{i\in\mathcal{K}\setminus\{k\}}\sum_{m'\in\mathcal{M}} \frac{\alpha_{im'} P_i G_{im}^{\mathrm{T}} G_{mi}^{\mathrm{R}}}{L_{im}^{\mathrm{A}} L_{im}^{\mathrm{F}}}, + \sum_{i\in\mathcal{K}\setminus\{k\}}\sum_{n'\in\mathcal{N}} \frac{\beta_{in'} P_i G_{im}^{\mathrm{T}} G_{mi}^{\mathrm{R}}}{L_{im}^{\mathrm{A}} L_{im}^{\mathrm{F}}}, \tag{6}$$

where $\boldsymbol{\alpha} = [\boldsymbol{\alpha}_1, \cdots, \boldsymbol{\alpha}_M]$ with $\boldsymbol{\alpha}_m = [\alpha_{1m}, \cdots, \alpha_{Km}]$, and $\boldsymbol{\beta} = [\boldsymbol{\beta}_1, \cdots, \boldsymbol{\beta}_N]$ with $\boldsymbol{\beta}_n = [\beta_{1n}, \cdots, \beta_{Kn}]$. Here, $\boldsymbol{\alpha}$ and $\boldsymbol{\beta}$ are the service mode selection and target vehicle association indicator matrices. $\alpha_{im} = 1$ indicates that vehicle i is selected

TABLE I
LIST OF MAIN NOTATION

Notation	Description	Notation	Description
$\mathcal{K}$	The set of service provider vehicles	$\mathcal{M}$	The set of communication target vehicles
$\mathcal{N}$	The set of sensing target vehicles	S_{km}	Received power at vehicle m from vehicle k
θ_k	Horizontal beamwidth of the antenna for vehicle k	φ_k	Vertical beamwidth of the antenna for vehicle k
G^{M}	The antenna gain of the main lobe	G^{S}	The antenna gain of the side lobes
G^{T}	The antenna gain of transmitter	G^{R}	The antenna gain of receiver
L^{A}_{km}	Absorption loss between vehicle k and vehicle m	$\tau(d_{km})$	Transmittance of the medium
L^{F}_{km}	Spreading loss between vehicle k and vehicle m	$\phi(f)$	Overall absorption coefficient of the medium
P_k	Transmit power of vehicle k	d_{km}	Distance between vehicle k and vehicle m
$I^{\mathrm{C}}_{km}(\boldsymbol{\alpha},\boldsymbol{\beta})$	Interference to the communication link $k \to m$	$I^{\mathrm{S}}_{kn}(\boldsymbol{\alpha},\boldsymbol{\beta})$	Interference to the sensing link $k \to n$
$\gamma^{\mathrm{C}}_{km}(\boldsymbol{\alpha},\boldsymbol{\beta})$	SINR of the communication link $k \to m$	$\gamma^{\mathrm{S}}_{kn}(\boldsymbol{\alpha},\boldsymbol{\beta})$	SINR of the sensing link $k \to n$
$R^{\mathrm{C}}_{km}(\boldsymbol{\alpha},\boldsymbol{\beta})$	Data rate of vehicle k transmitting data to vehicle m	P_k	Transmit power of vehicle k
B	Spectrum bandwidth	N_0	Johnson-Nyquist noise power
$\boldsymbol{\alpha}$	Target vehicle association indicator matrix for communication mode	$\boldsymbol{\beta}$	Target vehicle association indicator matrix for sensing mode
σ	Radar cross section (RCS)	f	Operating frequency
$\gamma_{\min}$	The Minimum SINR requirement of the sensing service	L^{S}_{kn}	Spreading loss of the path $k \to n \to k$
$\mathcal{G}$	Heterogeneous graph representation	$\mathcal{V}$	Node set of graph $\mathcal{G}$
$\mathcal{E}$	Edge set of graph $\mathcal{G}$	$\mathcal{O}$	Node type set of graph $\mathcal{G}$
$\mathcal{R}$	Edge type set of graph $\mathcal{G}$	$\boldsymbol{f}_v$	The feature of vehicle v
$g_{vv'}$	Weight of the edge between vehicle v and vehicle v'	Q	Total number of target vehicles
$\lvert\mathcal{K}\rvert$	The number of service provider vehicles	s_i	Sampling size of sampling iteration i
$\mathcal{L}^1(k)$	The set of the first hop vehicles for vehicle k	$\mathcal{L}^2(k)$	The set of the second hop vehicles for vehicle k
$\mathcal{L}^1_R(k)$	The subset of the first hop vehicles of vehicle k with the type R edge	λ_0	The dimension of graph information vector
$\sigma(\cdot)$	Rectified linear unit function (ReLU)	$\delta(\cdot)$	Sigmoid function
$J(\boldsymbol{w},\boldsymbol{p},\boldsymbol{b})$	Binary cross entropy (BCE) loss	$\boldsymbol{w},\boldsymbol{p},\boldsymbol{b}$	Weight matrices and bias of GNN
$\boldsymbol{h}^2_k$	Graph information of vehicle k	η	Learning rate
$\boldsymbol{y}_k$	Probability distribution of vehicle k serving each target vehicle	z^q_k	The label of vehicle k for class q

to serve vehicle m in the communication mode; otherwise, $\alpha_{im}=0$. Similarly, $\beta_{in}=1$ means that vehicle i is selected to detect vehicle n in the sensing mode; otherwise, $\beta_{in}=0$. In (6), the first term represents the interference from other SPVs that operate in the communication mode, while the second term is the interference from other SPVs that operate in the sensing mode.

The signal-to-interference-plus-noise ratio (SINR) for vehicle k transmitting to vehicle m is

$$\gamma^{\mathrm{C}}_{km}(\boldsymbol{\alpha},\boldsymbol{\beta})=\frac{\alpha_{km}S_{km}}{I^{\mathrm{C}}_{km}(\boldsymbol{\alpha},\boldsymbol{\beta})+N_{km}}, \tag{7}$$

where $N_{km}=N_0+\sum_{i\in\mathcal{K}\setminus\{k\}}P_iG^{\mathrm{T}}_{im}G^{\mathrm{R}}_{mi}(1-\tau(d_{im}))/L^{\mathrm{F}}_{im}$ with N_0 being the Johnson-Nyquist noise power. N_{km} is caused by the thermal agitation of electrons and molecular absorption.

Therefore, the data rate of vehicle k transmitting data to vehicle m is

$$R^{\mathrm{C}}_{km}(\boldsymbol{\alpha},\boldsymbol{\beta})=B\log_2\left(1+\gamma^{\mathrm{C}}_{km}(\boldsymbol{\alpha},\boldsymbol{\beta})\right), \tag{8}$$

where B denotes the channel bandwidth.

3) Sensing Mode: The interference to vehicle k operating in the sensing mode can be expressed as

$$I^{\mathrm{S}}_{kn}(\boldsymbol{\alpha},\boldsymbol{\beta})=\sum_{i\in\mathcal{K}\setminus\{k\}}\sum_{m'\in\mathcal{M}}\frac{\alpha_{im'}P_iG^{\mathrm{T}}_{ik}G^{\mathrm{R}}_{ki}}{L^{\mathrm{A}}_{ik}L^{\mathrm{F}}_{ik}}+\sum_{i\in\mathcal{K}\setminus\{k\}}\sum_{n'\in\mathcal{N}}\frac{\beta_{in'}P_iG^{\mathrm{T}}_{ik}G^{\mathrm{R}}_{ki}}{L^{\mathrm{A}}_{ik}L^{\mathrm{F}}_{ik}}$$

$$+\sum_{i\in\mathcal{K}\setminus\{k\}}\sum_{n'\in\mathcal{N}}\frac{\beta_{in'}P_iG^{\mathrm{T}}_{in}G^{\mathrm{R}}_{nk}\sigma_{in}c^2}{(4\pi)^3f^2d^2_{in}d^2_{kn}L^{\mathrm{A}}_{in}L^{\mathrm{A}}_{kn}}, \quad (9)$$

where σ_{in} is the target's radar cross section (RCS) between vehicle i and vehicle n. In (9), the first term represents the interference caused by other SPVs operating in the communication mode. The second term represents the interference caused by other SPVs operating in the sensing mode via direct path. The third term represents the interference caused by other SPVs operating in sensing mode via scattering paths.

From (6) and (9), we can see that a vehicle that operates in the sensing mode is interfered by other vehicles that operate in the sensing mode from scattering paths, which will not interfere the vehicles that operate in communication mode. This is because the impacts of scattered sensing signals on a communication link is much weaker than that on a sensing link [17].

Given (9), the SINR of vehicle k that operates in the sensing mode when sensing vehicle n can be expressed as

$$\gamma^{\mathrm{S}}_{kn}(\boldsymbol{\alpha},\boldsymbol{\beta})=\frac{\beta_{kn}P_kG^{\mathrm{T}}_{kn}G^{\mathrm{R}}_{nk}(L^{\mathrm{S}}_{kn})^{-1}(L^{\mathrm{A}}_{kn})^{-1}}{I^{\mathrm{S}}_{kn}(\boldsymbol{\alpha},\boldsymbol{\beta})+N_{kn}}, \quad (10)$$

where $L^{\mathrm{S}}_{kn}=\frac{(4\pi)^3f^2d^4_{kn}}{\sigma_{kn}c^2}$ is the spreading loss of the path $k\rightarrow n\rightarrow k$.

B. Problem Formulation

To maximize the data rates of all communication target vehicles while satisfying the sensing service requirements, an optimization problem is formulated as:

$$\max_{\boldsymbol{\alpha},\boldsymbol{\beta}} \quad \sum_{k\in\mathcal{K}}\sum_{m\in\mathcal{M}}R^{\mathrm{C}}_{km}(\boldsymbol{\alpha},\boldsymbol{\beta}) \quad (11)$$

$$\text{s.t.} \quad \sum_{k\in\mathcal{K}}\alpha_{km}=1,\alpha_{km}\in\{0,1\},\forall m\in\mathcal{M}, \quad (11a)$$

$$\sum_{k\in\mathcal{K}}\beta_{kn}=1,\beta_{kn}\in\{0,1\},\forall n\in\mathcal{N}, \quad (11b)$$

$$\sum_{m\in\mathcal{M}}\alpha_{km}\geq 0,\sum_{n\in\mathcal{N}}\beta_{kn}\geq 0,\forall k\in\mathcal{K}, \quad (11c)$$

$$\alpha_{km}\beta_{kn}=0,\forall k\in\mathcal{K},\forall m\in\mathcal{M},\forall n\in\mathcal{N}, \quad (11d)$$

$$\sum_{k\in\mathcal{K}}\gamma^{\mathrm{S}}_{kn}(\boldsymbol{\alpha},\boldsymbol{\beta})\geq\gamma_{\min},\forall n\in\mathcal{N}, \quad (11e)$$

where $\gamma_{\min}$ is the minimum SINR requirement of the sensing service. In (11), constraint (11a) ensures that a communication target vehicle can only be served by one SPV. Constraint (11b) ensures that a sensing target vehicle can only be detected by one SPV. Constraint (11c) indicates that an SPV can serve multiple communication or sensing target vehicles simultaneously. Constraint (11d) indicates that an SPV can operate in either the communication mode or the sensing mode, but not both simultaneously. Constraint (11e) is the minimum SINR requirement of the sensing service. From (11), we see that, increasing the number of target vehicles served by one SPV may increase the communication and sensing interference of other target vehicles served by other SPVs, which may reduce the overall data rates. Therefore, to maximize the overall data rates, the number of target vehicles served by each SPV should be limited.

Problem (11) is hard to solve due to the following reasons. First, the objective function is non-convex and hence the complexity of using traditional optimization algorithms will be extremely high. Second, traditional optimization algorithms require accurate channel information to obtain the free space path gain L^{F}_{km} and molecular absorption path gain L^{A}_{km} to solve problem (11). However, only periodically reported channel information can be obtained in highly dynamic THz-enabled vehicular networks. Third, traditional optimization methods do not consider the dynamic vehicle network topology such as the arrival of new vehicles. Therefore, when the vehicle topology changes, the central controller must execute the optimization algorithm again to re-optimize service mode selection and target vehicle associations. Machine learning (ML) can be developed to learn the relationship between neighborhood nodes rather than obtaining a separate feature vector for each vehicle [36], [37]. To solve the above formulated problem, we propose to use GNNs to generate the feature vector for each vehicle. Compared with other neural network methods such as multi-layer perceptrons (MLPs) and convolutional neural networks (CNNs) that can extract only geographical location information from a vehicle network topology, a GNN-based algorithm can extract not only geographical location information but also topological information. Meanwhile, a GNN can efficiently obtain the feature vector of a new vehicle without retraining, and then the new service mode selection and target vehicle association strategy can be explicitly determined based on the extracted feature vectors.

III. Service Mode Selection and Target Vehicle Association Based on GNN

In this section, we introduce a heterogeneous GNN-based algorithm to solve problem (11). First, we transform the joint service mode selection and target vehicle association problem (11) into a classification problem, where SPVs and target vehicles are considered as samples and classes, respectively. Since each SPV can simultaneously provide communication/sensing service for multiple communication/sensing target vehicles, the corresponding problem naturally becomes a multi-label classification problem, where each sample belongs to a set of classes. We study the use of a heterogeneous GNN-based algorithm to solve this classification problem. Compared to a homogeneous GNN-based algorithm that can only extract the features of a single type of vehicles, our designed heterogeneous GNN-based algorithm can extract vehicle topology features of several types of vehicles since it uses different weight matrices to represent the features of different type of vehicles. Next, we first introduce the use of a heterogeneous graph to represent the considered system model, and then introduce the components of our designed algorithm. Finally, we will explain the training method for the designed algorithm.

A. Graph Representation of Vehicular Networks

We first introduce the use of a heterogeneous graph to represent the considered vehicular network. A heterogeneous graph $\mathcal{G}=(\mathcal{V},\mathcal{E},\mathcal{O},\mathcal{R})$ consists of a node set $\mathcal{V}$, an edge set

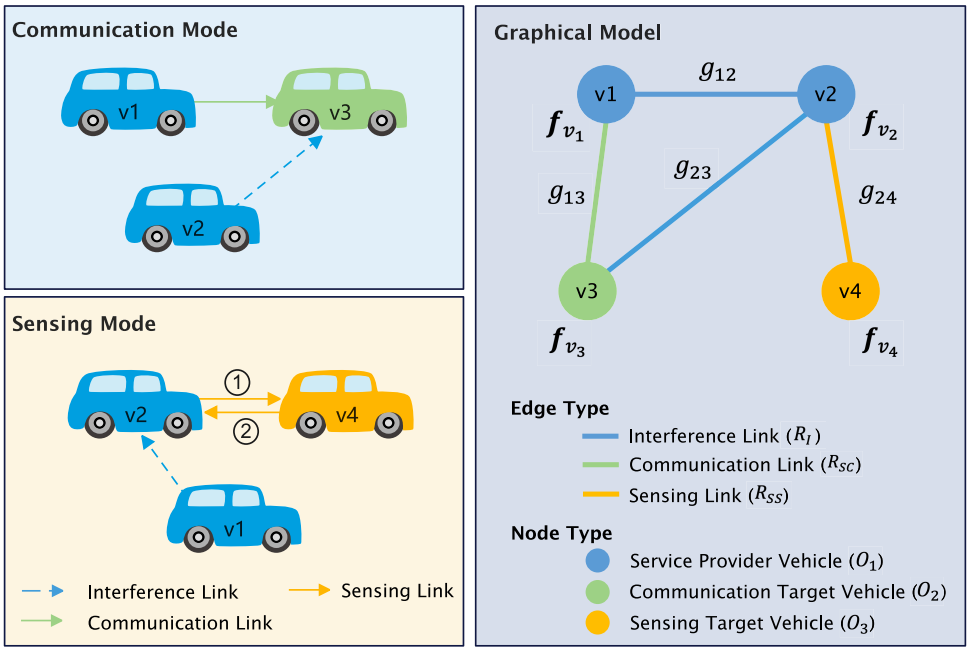

Fig. 2. Graph representation of the vehicular network.

$\mathcal{E}$, a node type set $\mathcal{O}$, and a set $\mathcal{R}$ that consists of different edge types. We model each vehicle as a node in the graph, and each link between two vehicles as an edge. The nodes can be divide into three categories, $\mathcal{O} = \{O_1, O_2, O_3\}$, which correspond to the three types of vehicles. Meanwhile, we consider three types of edges $\mathcal{R} = \{R_{SC}, R_{SS}, R_I\}$, where R_{SC} represents the communication link between an SPV and a communication target vehicle, R_{SS} represents the sensing link between an SPV and a sensing target vehicle, and R_I represents the interference link between two SPVs. By using the above graph representation, we can convert the considered vehicular network into a graphical model, as shown in Fig. 2. Specifically, the node feature of each vehicle is $\boldsymbol{f}_v = [e_{v1}, \ldots, e_{vM'}], v \in \mathcal{K} \cup \mathcal{M} \cup \mathcal{N}, \mathcal{M}' = \mathcal{M} \cup \mathcal{N}$, where $\boldsymbol{f}_v \in \mathbb{R}^{Q\times 1}$, $Q = (|\mathcal{M}| + |\mathcal{N}|)$ is the total number of target vehicles, and $e_{vm'}$ is the number of SPVs within the line-of-sight link between vehicle v and vehicle m', as shown in Fig. 3. The node feature evaluates the potential interference between the current vehicle and each target vehicle. The weight of the edge between vehicle v and vehicle v' is $g_{vv'} = \left(L^{\mathrm{A}}_{vv'} L^{\mathrm{F}}_{vv'}\right)^{-1}$ for all $v' \in \mathcal{V} \setminus \{v\}$ with $\boldsymbol{g}_{vv'} \in \mathbb{R}^{1\times 1}$.

B. Components of the GNN-Based Algorithm

A standard GNN model consists of two important modules, neighbor sampling module and feature updating module [38], [39], [40]. Neighbor sampling module is used to select the relevant neighborhood nodes for a given node. Feature updating module is used to generate the graph information vector for the given node by aggregating the graph information from the neighborhood nodes selected by the neighbor sampling module. Next, we will introduce the components of the proposed GNN-based solution

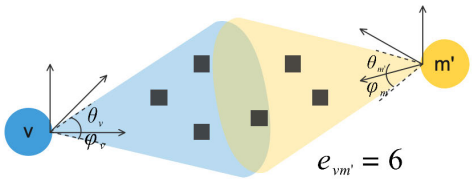

Fig. 3. An illustration of node feature.

for problem (11). Then, we will explain its training process.

The proposed GNN-based algorithm consists of six components: a) agent, b) input layer, c) hidden layer I, d) hidden layer II, e) hidden layers III-V, and f) output layer, which are specified as follows:

- *Agent*: The agent is a central controller that can obtain the geographic locations of all vehicles. In each time slot, the central controller implements the proposed GNN-based algorithm to determine the service mode and target vehicle association for each SPV. Therefore, the controller actually executes the neural network $|\mathcal{K}|$ times so as to determine the service mode and target vehicle association for the $|\mathcal{K}|$ vehicles.
- *Input Layer*: To determine the service mode of vehicle k and its serviced vehicles, the input of the designed scheme is based on the features of the vehicles that can connect to vehicle k. However, since the number of vehicles that can connect to different SPVs are varying, the size of the input matrix may also be different. To enable a neural network to extract graph information for different SPVs that may connect to different number of service target vehicles, we use uniform sampling to calculate the average features of each connected vehicle so as to fix

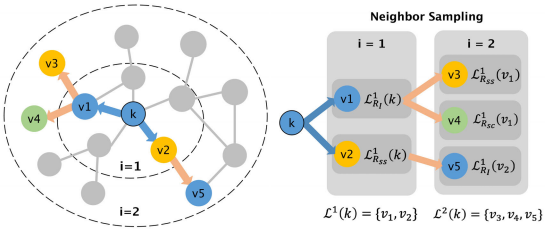

Fig. 4. Aggregate feature information from neighbors.

the size of the input. In particular, we assume that the number of vehicles that the proposed algorithm needs to sample for a vehicle k is s_i in sampling iteration $i \in \{1, \cdots, I\}$. Meanwhile, we assume that the set of sampled vehicles that can directly connect to vehicle k as the set of the first hop vehicles, which is represented by $\mathcal{L}^1(k)$ with $|\mathcal{L}^1(k)| = s_1$ being the number of vehicles in set $\mathcal{L}^1(k)$. The set of sampled vehicles that can connect to vehicle k via the first hop vehicles as the set of the second hop vehicles represented by $\mathcal{L}^2(k)$, where $\mathcal{L}^2(k) = \{\mathcal{L}^1(v') | v' \in \mathcal{L}^1(k)\}$. The number of vehicles in set $\mathcal{L}^2(k)$ is s_2. For example, in Fig. 4, the total number of sampled vehicles is 5 ($s_1 = 2$ and $s_2 = 3$), $\mathcal{L}^1(k) = \{v_1, v_2\}$, and $\mathcal{L}^2(k) = \{v_3, v_4, v_5\}$. We assume that the subset of the first hop vehicles with a type R edge is $\mathcal{L}^1_R(k)$. For example, in Fig. 4, $\mathcal{L}^1_{R_I}(k) = \{v_1\}$ and $\mathcal{L}^1_{R_{SS}}(k) = \{v_2\}$. Given these definitions, we next introduce the input of the proposed GNN-based method. From Fig. 5, we see that the input is connected to four fully connected layers and each fully connected layer has different inputs. The inputs to the four fully connected layers are: i) $\boldsymbol{h}^0_k = \boldsymbol{f}_k \in \mathbb{R}^{Q\times 1}$, ii) $\boldsymbol{h}^1_{R_{SC}} \in \mathbb{R}^{(Q+1)\times 1}$, iii) $\boldsymbol{h}^1_{R_{SS}} \in \mathbb{R}^{(Q+1)\times 1}$, and iv) $\boldsymbol{h}^1_{R_I} \in \mathbb{R}^{(Q+1)\times 1}$, where

$$\boldsymbol{h}^1_{R_{SC}} = \frac{1}{|\mathcal{L}^1_{R_{SC}}(k)|} \sum_{v' \in \mathcal{L}^1_{R_{SC}}(k)} \boldsymbol{h}^0_{kv'}, \tag{12}$$

$$\boldsymbol{h}^1_{R_{SS}} = \frac{1}{|\mathcal{L}^1_{R_{SS}}(k)|} \sum_{v' \in \mathcal{L}^1_{R_{SS}}(k)} \boldsymbol{h}^0_{kv'}, \tag{13}$$

$$\boldsymbol{h}^1_{R_I} = \frac{1}{|\mathcal{L}^1_{R_I}(k)|} \sum_{v' \in \mathcal{L}^1_{R_I}(k)} \boldsymbol{h}^0_{kv'}, \tag{14}$$

with $\boldsymbol{h}^0_{kv'} = [\boldsymbol{h}^0_{v'} \| g_{kv'}]$, $\boldsymbol{h}^0_{kv'} \in \mathbb{R}^{(Q+1)\times 1}$, $\cdot\|\cdot$ representing the vector concatenation operation, $|\mathcal{L}^1_{R_{SC}}(k)|$, $|\mathcal{L}^1_{R_{SS}}(k)|$, and $|\mathcal{L}^1_{R_I}(k)|$ being the number of vehicles in set $\mathcal{L}^1_{R_{SC}}(k)$, $\mathcal{L}^1_{R_{SS}}(k)$, and $\mathcal{L}^1_{R_I}(k)$, respectively. Here, (12)-(14) are the neighbor sampling module of the designed GNN model. In (12)-(14), we use a neighborhood information averaging approach for the extraction of neighborhood vehicle features since it has a low computational complexity but can achieve a similar performance with the method that uses a neural network layer (e.g., LSTM) to aggregate the neighborhood vehicle information [41]. In future, we will design more effective neighborhood sampling methods.

- *Hidden Layer I*: This layer consists of four fully-connected layers and it is used to extract the graph information of the first hop vehicles of each vehicle k. The output of this layer is

$$\boldsymbol{h}^1_k = \sigma\left([\boldsymbol{w}_1 \boldsymbol{h}^0_k \| \boldsymbol{w}_2 \boldsymbol{h}^1_{R_{SC}} \| \boldsymbol{w}_3 \boldsymbol{h}^1_{R_{SS}} \| \boldsymbol{w}_4 \boldsymbol{h}^1_{R_I}]\right), \tag{15}$$

where $\sigma(\cdot)$ is the rectified linear unit function (ReLU), $\boldsymbol{w}_1 \in \mathbb{R}^{(\lambda_0/4)\times Q}$, $\boldsymbol{w}_2 \in \mathbb{R}^{(\lambda_0/4)\times(Q+1)}$, $\boldsymbol{w}_3 \in \mathbb{R}^{(\lambda_0/4)\times(Q+1)}$, and $\boldsymbol{w}_4 \in \mathbb{R}^{(\lambda_0/4)\times(Q+1)}$ are the weights of the four fully connected layers, λ_0 is the dimension of the graph information vector, $\boldsymbol{w}_1$ is the weight matrix of the current vehicle, and $\boldsymbol{w}_2$, $\boldsymbol{w}_3$, and $\boldsymbol{w}_4$ are the weight matrices for the vehicles with the type R_{SC}, R_{SS}, and R_I edge, respectively. Here, (15) is the feature updating module of the designed GNN model. To support heterogeneous nodes and edges, we set separate neighbourhood weight matrices $\boldsymbol{w}_2$, $\boldsymbol{w}_3$, and $\boldsymbol{w}_4$ for each type of vehicles, respectively. From (12) to (15), we extract only the graph information of vehicle v. However, we need the graph information of all the sampled first hop vehicles to optimize service mode selection and vehicle connection. Therefore, we need to execute (12) to (15) for each sampled vehicle (i.e., for s_1 times). After that, we obtain $\boldsymbol{h}^1_{v'} \in \mathbb{R}^{\lambda_0\times 1}$, $\forall v' \in \mathcal{L}^1(k)$ for each sampled vehicle v'.
- *Hidden Layer II*: This layer consists of four fully-connected layers and it is used to extract the graph information of the second hop vehicles of vehicle k. From Fig. 5, we can see that the input to each fully connected layer in hidden layer II is different. The inputs to the four fully connected layers are: i) $\boldsymbol{h}^1_k \in \mathbb{R}^{\lambda_0\times 1}$, ii) $\boldsymbol{h}^2_{R_{SC}} \in \mathbb{R}^{(\lambda_0+1)\times 1}$, iii) $\boldsymbol{h}^2_{R_{SS}} \in \mathbb{R}^{(\lambda_0+1)\times 1}$, and iv) $\boldsymbol{h}^2_{R_I} \in \mathbb{R}^{(\lambda_0+1)\times 1}$, where

$$\boldsymbol{h}^2_{R_{SC}} = \frac{1}{|\mathcal{L}^1_{R_{SC}}(k)|} \sum_{v' \in \mathcal{L}^1_{R_{SC}}(k)} \boldsymbol{h}^1_{kv'}, \tag{16}$$

$$\boldsymbol{h}^2_{R_{SS}} = \frac{1}{|\mathcal{L}^1_{R_{SS}}(k)|} \sum_{v' \in \mathcal{L}^1_{R_{SS}}(k)} \boldsymbol{h}^1_{kv'}, \tag{17}$$

$$\boldsymbol{h}^2_{R_I} = \frac{1}{|\mathcal{L}^1_{R_I}(k)|} \sum_{v' \in \mathcal{L}^1_{R_I}(k)} \boldsymbol{h}^1_{kv'}, \tag{18}$$

with $\boldsymbol{h}^1_{kv'} = [\boldsymbol{h}^1_{v'} \| g_{kv'}]$ and $\boldsymbol{h}^1_{kv'} \in \mathbb{R}^{(\lambda_0+1)\times 1}$. The output of this layer is

$$\boldsymbol{h}^2_k = \sigma\left([\boldsymbol{w}_5 \boldsymbol{h}^1_k \| \boldsymbol{w}_6 \boldsymbol{h}^2_{R_{SC}} \| \boldsymbol{w}_7 \boldsymbol{h}^2_{R_{SS}} \| \boldsymbol{w}_8 \boldsymbol{h}^2_{R_I}]\right), \tag{19}$$

where $\boldsymbol{h}^2_k \in \mathbb{R}^{\lambda_0\times 1}$, $\boldsymbol{w}_5 \in \mathbb{R}^{(\lambda_0/4)\times\lambda_0}$, $\boldsymbol{w}_6 \in \mathbb{R}^{(\lambda_0/4)\times(\lambda_0+1)}$, $\boldsymbol{w}_7 \in \mathbb{R}^{(\lambda_0/4)\times(\lambda_0+1)}$, and $\boldsymbol{w}_8 \in \mathbb{R}^{(\lambda_0/4)\times(\lambda_0+1)}$ are the weights of the four fully connected layers, respectively. $\boldsymbol{w}_5$ is the weight matrix of vehicle k and the others are the weight matrices for the three types of second hop vehicles, i.e., $\boldsymbol{w}_6$ is the weight matrix for the vehicles with a type R_{SC} edge, $\boldsymbol{w}_7$ is the weight matrix for the vehicles with a type R_{SS} edge, and $\boldsymbol{w}_8$ is the weight matrix for the vehicles with a type R_I edge. Compared to the aggregate function in [41] and [42] that considers only node features, we consider both node features and edge weights in both hidden layers I and II. Here, the output $\boldsymbol{h}^2_k$ can be considered as the graph information of vehicle k, since it includes the

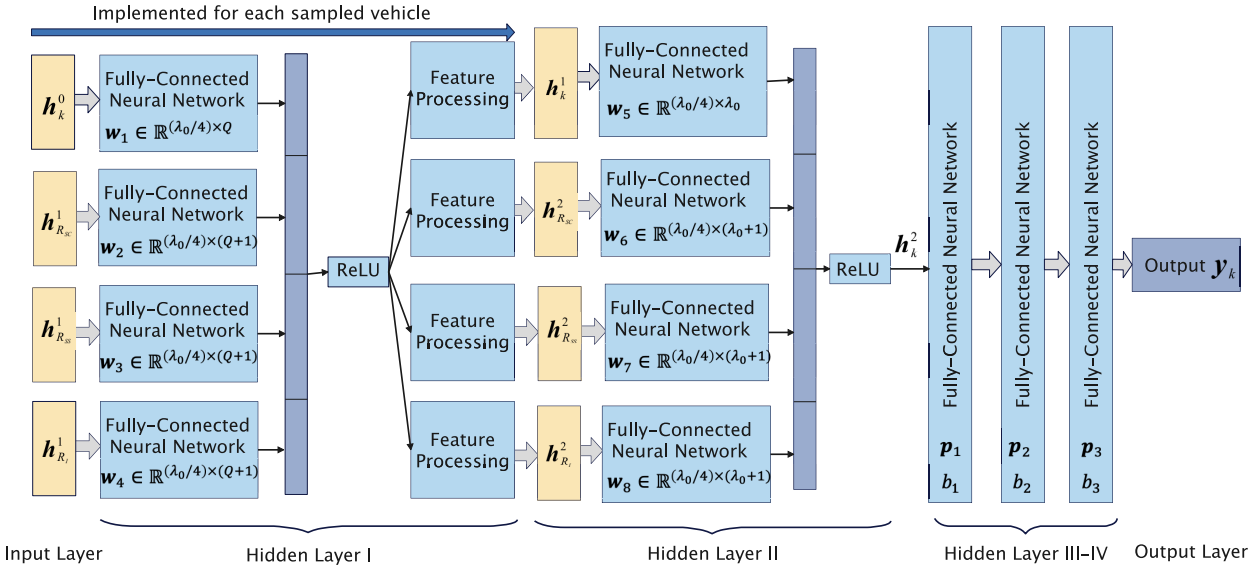

Fig. 5. Structure of the proposed GNN model.

graph information of the sampled first hop and second hop vehicles. (16)-(18) are the neighor sampling module of the designed GNN model while (19) is the feature updating module.

- *Hidden Layers III-V*: Three fully-connected layers are used to find the relationship between the graph information vector $\boldsymbol{h}_k^2$ and the probability distribution of vehicle k serving each target vehicle in the corresponding operating mode.
- *Output*: The output of the network, $\boldsymbol{y}_k = \left[y_k^1, \cdots, y_k^{Q+1}\right]$, is the probability distribution of vehicle k serving $Q+1$ target vehicles in the corresponding operating mode. Here, $Q+1$ is the total number of classification classes, including the case that vehicle k is not connected to any target vehicles.

C. Training the Proposed GNN-Based Model

Given the components defined in the previous section, we next introduce the entire procedure of training the proposed GNN-based method. We use binary cross entropy (BCE) as the loss function to minimize the difference between the predicted multi-label classification result and the actual multi-label classification result, which is given by:

$$J\left(\boldsymbol{w},\boldsymbol{p},\boldsymbol{b}\right) = \sum_{q=1}^{Q+1} -z_k^q \log\delta\left(y_k^q\right) - \left(1-z_k^q\right)\log\left(1-\delta\left(y_k^q\right)\right), \tag{20}$$

where $\delta\left(\cdot\right)$ is the sigmoid function; z_k^q is the label of vehicle k for class q, which is generated by exhaustive searching; $\boldsymbol{w}$ is the weight matrix of hidden layer I; and $\boldsymbol{p}$ and $\boldsymbol{b}$ are the weight matrix and bias of hidden layer III-V, respectively. To minimize the training loss (11), we optimize $\boldsymbol{w}$, $\boldsymbol{p}$, and $\boldsymbol{b}$ using the back-propagation algorithm with the mini-batch stochastic gradient descent (SGD) approach [41]. The parameters of each fully-connected layer j in the GNN, i.e., $\boldsymbol{w}_j$, $\boldsymbol{p}_{j'}$, and $\boldsymbol{b}_{j'}$, are randomly initialized by a uniform distribution and updated by the central controller in each training iteration $t \in \{1, \cdots, T\}$ of the mini-batch SGD approach, where T is the number of total training iterations. Specifically, the standard update policy of mini-batch SGD is given by:

$$\boldsymbol{w}_j^{t+1} = \boldsymbol{w}_j^t - \eta\frac{1}{|\mathcal{B}|}\sum_{k\in\mathcal{B}_t}\frac{\partial J\left(\boldsymbol{w},\boldsymbol{p},\boldsymbol{b}\right)}{\partial \boldsymbol{w}_j}, \tag{21}$$

$$\boldsymbol{p}_{j'}^{t+1} = \boldsymbol{p}_{j'}^t - \eta\frac{1}{|\mathcal{B}|}\sum_{k\in\mathcal{B}_t}\frac{\partial J\left(\boldsymbol{w},\boldsymbol{p},\boldsymbol{b}\right)}{\partial \boldsymbol{p}_{j'}}, \tag{22}$$

$$\boldsymbol{b}_{j'}^{t+1} = \boldsymbol{b}_{j'}^t - \eta\frac{1}{|\mathcal{B}|}\sum_{k\in\mathcal{B}_t}\frac{\partial J\left(\boldsymbol{w},\boldsymbol{p},\boldsymbol{b}\right)}{\partial \boldsymbol{b}_{j'}}, \tag{23}$$

where $|\mathcal{B}|$ is the size of mini-batches, $\mathcal{B}_t$ is a mini-batch of training samples used in iteration t, η is the learning rate, $j \in \{1,2,3,4,5,6,7,8\}$, and $j' \in \{1,2,3\}$. $\boldsymbol{w}_j, \forall j \in \{1,2,3,4\}$ is the weight matrix of fully-connected layer j in hidden layer I. $\boldsymbol{w}_j, \forall j \in \{5,6,7,8\}$ is the weight matrix of fully-connected layer j in hidden layer II. $\boldsymbol{p}_{j'}, \forall j' \in \{1,2,3\}$ and $b_{j'}, \forall j' \in \{1,2,3\}$ are the weight matrix and bias of fully-connected layer j' in hidden layer III-V. The entire training process of the proposed GNN-based algorithm is summarized in **Algorithm 1**.

D. Solution for the Formulated Problem

Once the probability distribution $\boldsymbol{y}_k$ of each SPV k is obtained, the service mode selection and target vehicle association can be determined. In particular, given $\boldsymbol{y}_k$, the objective function in (11) can be approximated by

$$E(\boldsymbol{\alpha},\boldsymbol{\beta}) = \sum_{m\in\mathcal{M}}\sum_{k\in\mathcal{K}}\alpha_{km}y_k^m + \sum_{n\in\mathcal{N}}\sum_{k\in\mathcal{K}}\beta_{kn}y_k^{|\mathcal{M}|+n}, \tag{24}$$

where the first term $\sum_{m\in\mathcal{M}}\sum_{k\in\mathcal{K}}\alpha_{km}y_k^m$ is the sum of the probabilities of establishing all the communication links, and the second term $\sum_{n\in\mathcal{N}}\sum_{k\in\mathcal{K}}\beta_{kn}y_k^{|\mathcal{M}|+n}$ represents the sum of the probabilities of establishing all the sensing links.

Algorithm 1 GNN-Based Method for the Joint Service Mode Selection and Target Vehicle Association Problem

Input: Vehicle features $\{\boldsymbol{f}_v, \forall v \in \mathcal{V}\}$, edge weights $\{g_{vv'}, \forall v' \in \mathcal{V} \setminus \{v\}\}$, and sampling size s_1 and s_2;
Initialize: $\boldsymbol{w}_j$, $\boldsymbol{p}_{j'}$, and $b_{j'}$;
$\boldsymbol{h}_v^0 \leftarrow \boldsymbol{f}_v$, $\boldsymbol{h}_{vv'}^0 \leftarrow \left[\boldsymbol{h}_{v'}^0 \| g_{vv'}\right]$, $\forall v \in \mathcal{V}, \forall v' \in \mathcal{V} \setminus \{v\}$;
for $k = 1 \rightarrow K$ **do**
  Sample the first hop vehicles $\mathcal{L}^1(k)$ and second hop vehicles $\mathcal{L}^2(k)$ for vehicle k;
  Extract the graph information $\boldsymbol{h}_k^1$ of vehicle k based on (12)-(15);
  for $v' \in \mathcal{L}^1(k)$ **do**
    Extract the graph information $\boldsymbol{h}_{v'}^1$ of vehicle v' based on (12)-(15);
  end for
  $\boldsymbol{h}_{kv'}^1 \leftarrow [\boldsymbol{h}_{v'}^1 \| g_{kv'}]$, $\forall v' \in \mathcal{L}^1(k)$;
  Aggregate the neighborhood feature vectors of vehicle k, $\boldsymbol{h}_{R_{SC}}^2$, $\boldsymbol{h}_{R_{SS}}^2$, and $\boldsymbol{h}_{R_I}^2$, based on (16)-(18);
  Concatenate the vehicle's current representation, $\boldsymbol{h}_k^1$, with the aggregated neighborhood vector based on (19);
  Obtain the graph information vector $\boldsymbol{h}_k^2$ for vehicle k;
  Use $\boldsymbol{h}_k^2$ as input to predict the probability distribution $\boldsymbol{y}_k$ of vehicle k;
  Calculate loss $J(\boldsymbol{w}, \boldsymbol{p}, \boldsymbol{b})$ based on (20);
  Update the weight matrices and bias using (21)-(23);
end for
Output: The probability distribution $\boldsymbol{y}_k$ for each vehicle $k \in \mathcal{K}$.

Here, a small gap may exist between the original objective function in (11) and the approximated objective function in (24). However, this approximation can significantly simplify the solution procedure for determining service mode selection and target vehicle association. We will use simulation results in Section IV to verify the accuracy of this approximation process. Given (24), the problem in (11) can be rewritten as

$$\max_{\boldsymbol{\alpha},\boldsymbol{\beta}} \quad E(\boldsymbol{\alpha}, \boldsymbol{\beta}) \tag{25}$$

$$\text{s.t.} \quad \sum_{k\in\mathcal{K}} \alpha_{km} = 1, \alpha_{km} \in \{0,1\}, \forall m \in \mathcal{M}, \tag{25a}$$

$$\sum_{k\in\mathcal{K}} \beta_{kn} = 1, \beta_{kn} \in \{0,1\}, \forall n \in \mathcal{N}, \tag{25b}$$

$$\sum_{m\in\mathcal{M}} \alpha_{km} \geq 0, \sum_{n\in\mathcal{N}} \beta_{kn} \geq 0, \forall k \in \mathcal{K}, \tag{25c}$$

$$\alpha_{km}\beta_{kn} = 0, \forall k \in \mathcal{K}, \forall m \in \mathcal{M}, \forall n \in \mathcal{N}, \tag{25d}$$

$$\sum_{k\in\mathcal{K}} \gamma_{kn}^{\mathrm{S}}(\boldsymbol{\alpha}, \boldsymbol{\beta}) \geq \gamma_{\min}, \forall n \in \mathcal{N}. \tag{25e}$$

In (25), constraints (25d) and (25e) are non-linear. Therefore, we need to rewrite and linearize these two constraints. For constraint (25d), we can rewrite it as $\alpha_{km} + \beta_{kn} \leq 1$, which guarantees that a service provider vehicle can only operate in either the communication mode or the sensing mode. For constraint (25e), since a sensing target vehicle n can only be connected with one service provider vehicle k, i.e., $\sum_{k\in\mathcal{K}} \gamma_{kn}^{\mathrm{S}}(\boldsymbol{\alpha}, \boldsymbol{\beta}) = \gamma_{kn}^{\mathrm{S}}(\boldsymbol{\alpha}, \boldsymbol{\beta})$ when $\beta_{kn} = 1$, we have $\gamma_{kn}^{\mathrm{S}}(\boldsymbol{\alpha}, \boldsymbol{\beta}) \geq \beta_{kn}\gamma_{\min}$.

Given the rewritten constraints (25d) and (25e), the optimization problem in (24) is now given by

$$\max_{\boldsymbol{\alpha},\boldsymbol{\beta}} \quad E(\boldsymbol{\alpha}, \boldsymbol{\beta}) \tag{26}$$

$$\text{s.t.} \quad (25a) - (25c), \tag{26a}$$

$$\alpha_{km} + \beta_{kn} \leq 1, \forall k \in \mathcal{K}, \forall m \in \mathcal{M}, \forall n \in \mathcal{N}, \tag{26b}$$

$$\gamma_{kn}^{\mathrm{S}}(\boldsymbol{\alpha}, \boldsymbol{\beta}) \geq \beta_{kn}\gamma_{\min}, \forall k \in \mathcal{K}, \forall n \in \mathcal{N}. \tag{26c}$$

Problem (26) is a quadratically constrained programming (QCP) problem. Thus, it can be solved by using a convex optimization tool, such as Gurobi [34].

E. Implementation of the Proposed GNN-Based Algorithm

Next, we analyze the implementation of the GNN-based algorithm. To implement the GNN-based algorithm for finding the optimal service mode selection and target vehicle association matrices $\boldsymbol{\alpha}$ and $\boldsymbol{\beta}$, the central controller must first obtain the vehicle topology. The vehicle topology is constructed based on the vehicles' periodically reported GPS data. Then, we need to transform the vehicle topology into the heterogeneous graph representation. To establish the heterogeneous graph representation, the central controller must know 1) the path loss (i.e., the spreading loss and the absorption loss) between each two vehicles $v, v' \in \mathcal{V}$ to obtain the edge feature $g_{vv'}$, and 2) the antenna direction between each vehicle $v \in \mathcal{V}$ and each service target vehicle $m' \in \mathcal{M}'$ to obtain the node feature $\boldsymbol{f}_v$. The central controller can use channel estimation methods to learn the path loss and the antenna direction of each pair of vehicles [43]. Based on the heterogeneous graph representation, a GNN is used to determine the probability distribution $\boldsymbol{y}_k$ for each SPV. Given $\boldsymbol{y}_k$, the convex optimization tool can be used to find the optimal service mode selection and target vehicle association matrices $\boldsymbol{\alpha}$ and $\boldsymbol{\beta}$. Since the optimization function in (26) is convex, it will finally find the optimal $\boldsymbol{\alpha}$ and $\boldsymbol{\beta}$.

The proposed GNN-based algorithm includes an offline training phase and an online decision making phase. A well trained GNN model is transferred from the offline phase to the online phase. In the offline phase, the model is trained during the idle time of the central controller leveraging the historical geographic locations and network topological information. When the GNN model is well trained, a series of reasonable weights that can accurately map an input to an output are obtained. During the online decision making phase, the trained weights can be directly used for generating the probability distribution of each SPV without updating the weights of GNNs.

F. Complexity Analysis

Next, we analyze the computational complexity of the proposed GNN-based scheme for service mode selection and target vehicle association optimization. The complexity of the proposed scheme is analyzed from two parts: 1) complexity for training GNN-based scheme and 2) complexity for inference. The training process of the proposed GNN model is conducted

once in the offline training phase, while the inference process of determining the service mode of each service provider vehicle and target vehicle association is conducted for each vehicle topology.

1) Complexity for Training GNN-Based Scheme: The complexity for training GNN-based scheme lies in computing the graph information vector and performing multi-label classification. The computational complexity for graph information vector computation depends on the size of neighbor sampling s_i, the number of sampling iteration I, the dimension of graph information vector λ_0, and the number of SPVs $|\mathcal{K}|$. Hence, the computational complexity for graph information vector computation is given by $\mathcal{O}\left(\lambda_0|\mathcal{K}|\prod_{i=1}^{I} s_i\right)$. According to [44], the complexity of training a neural network depends on its width, depth, and number of parameters. The complexity of training hidden layer III-V to perform multi-label classification is $\mathcal{O}\left(\prod_{j=3}^{J} H_j\right)$, where H_j is the number of the neurons in layer j and J is the number of hidden layers. Therefore, the computational complexity for training GNN-based scheme is given by

$$\mathcal{O}\left(\left(\lambda_0|\mathcal{K}|\prod_{i=1}^{I} s_i\right)\prod_{j=3}^{J} H_j\right). \tag{27}$$

2) Complexity for Inference: The complexity for inference lies in determining the service mode selection and target vehicle association strategy based on the multi-label classification results. To solve problem (26), the computational complexity for determining the service mode selection and target vehicle association matrices is $\mathcal{O}\left(C|\mathcal{K}||\mathcal{M}||\mathcal{N}|\right) \approx \mathcal{O}\left(|\mathcal{K}||\mathcal{M}||\mathcal{N}|\right)$, where C denotes the number of multiplications per search step. It can be seen that given the structure of the proposed GNN-based model (i.e., s_i, H_j, λ_0, and I), the complexity of inference depends on the number of SPVs, the number of communication target vehicles, and the number of sensing target vehicles.

IV. Simulation Results and Analysis

In this section, we perform extensive simulations to evaluate the performance of our proposed scheme in a specific region of 100 m $\times$ 100 m. The other detailed parameters are listed in Table II [23], [24]. The GPS dataset used to generate vehicle topologies is obtained from Shanghai Traffic Department, which consists of ID, timestamp, latitude and longitude information of 18,900 vehicles [45]. We first select a specific region of 100 m $\times$ 100 m in Shanghai, which includes three main streets, as shown in Fig. 6. Then, we collect 3,500 vehicle topologies within this region. The time interval between two vehicle topologies is 30 seconds. Among these 3,500 vehicle topologies, 1,500 vehicle topologies are considered as a training dataset, 1,000 vehicle topologies are considered as a testing dataset, and 1,000 vehicle topologies are considered as a validation dataset. For comparison purposes, we consider three baselines. Baseline a is an exhaustive search algorithm, which can be considered as the optimal solution for problem (11). Baseline b is based on homogeneous graph. For a fair comparison, Baseline b uses the same neural network architecture as the proposed method, but a different graph information extraction method given in [30], where different types of nodes and edges are not distinguished. Baseline c directly uses the geographic location information to optimize service mode selection and target vehicle association scheme, without using GNNs to extract the graph information vectors.

TABLE II
System Parameters

Parameters	Value	Parameters	Value
c	3×10^8 m/s	f	1.05 THz
P	40 dBm	B	5 GHz
N_0	-77 dBm	$\phi(f)$	0.07512 m^{-1}
ε	0.1	θ, φ	10°, 10°
σ	1	$\gamma_{\min}$	3 dB
λ_0	64	η	0.7
s_1	10	s_2	10
I	2	T	20,000
Number of training vehicle topologies			1,500
Number of testing vehicle topologies			1,000
Number of validating vehicle topologies			1,000
Size of hidden layer III-V			32, 64, 64
Size of mini-batches $\|\mathcal{B}\|$			64

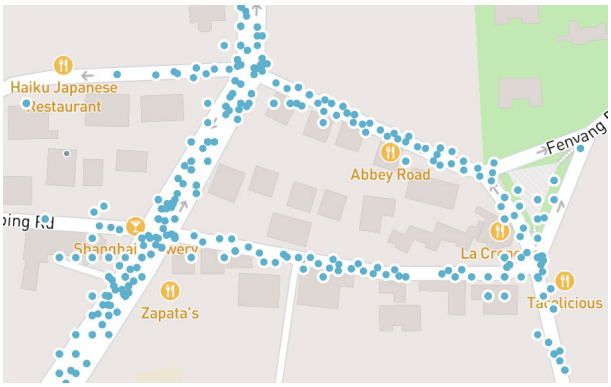

Fig. 6. Visualization of the GPS data.

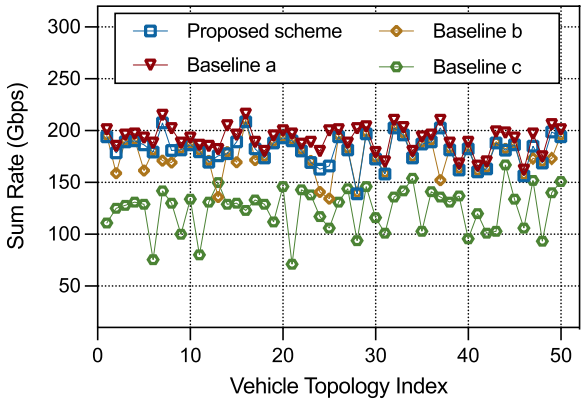

Fig. 7. The sum rate as the vehicle topology varies ($|\mathcal{K}| = 5$, $|\mathcal{M}| = 2$, and $|\mathcal{N}| = 2$).

Fig. 7 shows how the sum of data rates of all communication target vehicles change as the vehicle topology varies. In this figure, different indexes represent different non time-dependent vehicle topologies. From Fig. 7, we see that the proposed scheme improves the sum rate by up to 3.16% and 31.86% compared to baselines b and c. The 3.16% gain stems

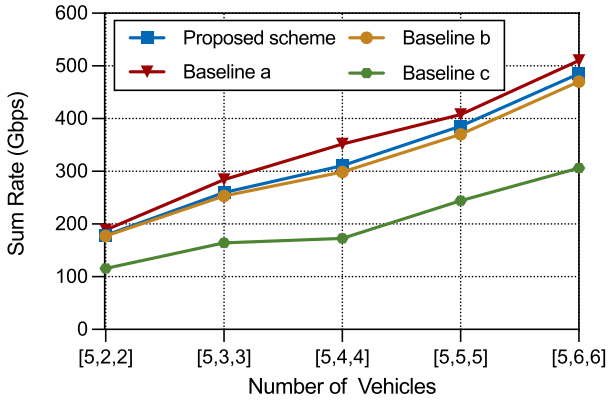

Fig. 8. The sum rate as the number of target vehicles varies ($|\mathcal{K}| = 5$, $|\mathcal{M}|$ and $|\mathcal{N}|$ vary from 2 to 6).

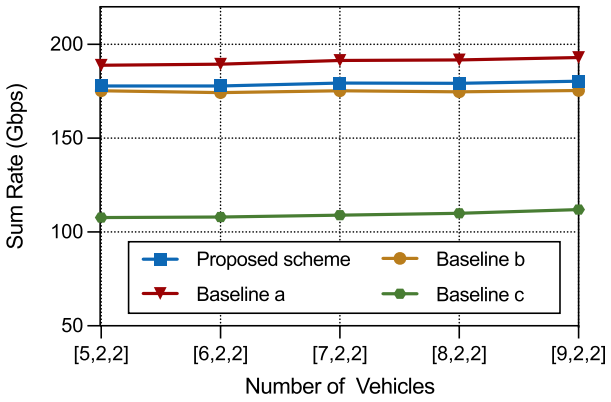

Fig. 9. The sum rate as the number of SPVs varies ($|\mathcal{M}| = |\mathcal{N}| = 2$ and $|\mathcal{K}|$ varies from 5 to 9).

from the fact that the proposed scheme uses a heterogeneous graph to represent a vehicle topology, hence, the impact of different types of vehicles on service mode selection and target vehicle association is considered. The 31.86% gain stems from the fact that the proposed scheme uses a GNN to extract a graph information vector for each SPV. In Fig. 7, we can also observe that, there is only a small performance gap between the proposed scheme and baseline a, which verifies the high approximation accuracy of (26).

Fig. 8 shows how the sum of data rates of all communication target vehicles changes as the number of communication and sensing target vehicles varies. From this figure, we can see that, as the number of communication and sensing target vehicles increases, the sum of data rates of all communication target vehicles increases since more communication links are established. Fig. 8 also shows that, compared to baselines b and c, the proposed scheme can achieve up to 2.94% and 35.45% gains in terms of the sum rate of all communication target vehicles. The 2.94% gain stems from the fact that the proposed scheme considers the use of heterogeneous GNNs to extract geographical location information and topological information from different types of vehicles. The 35.45% gain stems from the fact that the proposed scheme determines the target vehicle association based on the learned graph information vector and hence, it optimizes target vehicle association while considering all vehicle's location, connection, and communication interference. Fig. 8 also shows that the gap between the proposed scheme and baseline a is less than 7%. This indicates that the proposed GNN-based scheme enables the trained GNN to adapt to different vehicle topologies with different number of vehicles.

Fig. 9 shows how the sum of data rates of all communication target vehicles changes as the number of SPVs varies. From this figure, we can see that, as the number of SPVs increases, the sum of data rates of all communication target vehicles increases. This is due to the fact that the increase of the number of SPVs makes more SPVs available for communication target vehicles to select. In consequence, the communication target vehicles are more likely to select the SPVs with an appropriate direction and distance. Fig. 9 also shows that, compared to baseline c, the proposed scheme can achieve up to 36.45%

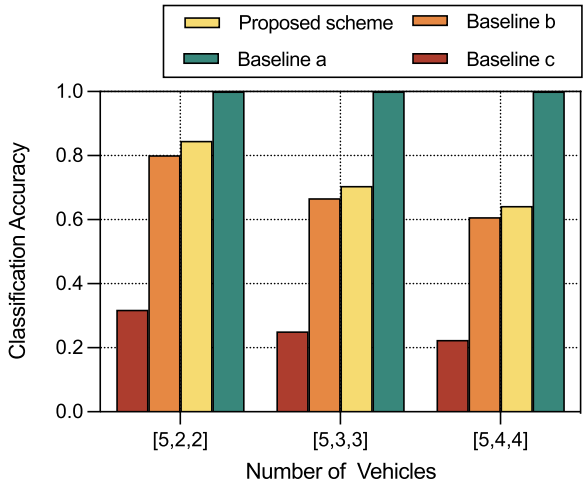

Fig. 10. The classification accuracy as the number of target vehicles varies ($|\mathcal{K}|$=5, $|\mathcal{M}|$ and $|\mathcal{N}|$ varies from 2 to 4).

gain in terms of sum rate. This is because the proposed algorithm considers both geographical location information and topological information. In Fig. 9, we can also see that the proposed scheme can achieve up to 2.06% gain in terms of sum rate compared to baseline b. This is due to the fact that the proposed algorithm uses heterogeneous GNN to learn the information of different types of vehicles.

Fig. 10 shows how the classification accuracy changes as the number of communication and sensing target vehicles varies. From this figure, we can see that, as the number of communication and sensing target vehicles increases, the classification accuracy resulting from all considered algorithms decreases. This is due to the fact that each SPV may now serve more target vehicles simultaneously. As the number of target vehicles increases, the interference among different vehicles increases and the connections among different vehicles become more complicated. Fig. 10 also shows that, compared to baseline c, the proposed scheme can achieve up to 46.77% gain in terms of classification accuracy. The reason is that the proposed scheme use GNNs to extract the graph information vectors, which can capture the location, connection, and interference information between vehicles. In Fig. 10, we can also see that the proposed scheme can

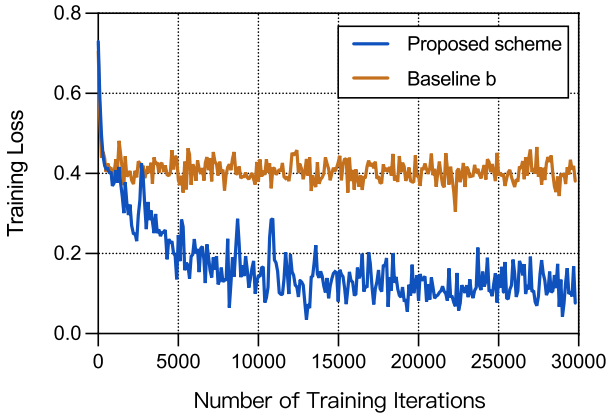

Fig. 11. The training loss as the number of training iterations varies.

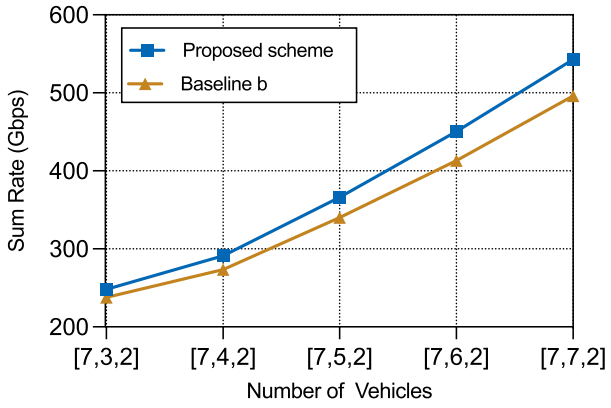

Fig. 12. The sum rate as the number of communication target vehicles varies ($|\mathcal{K}| = 7$, $|\mathcal{N}| = 2$, and $|\mathcal{M}|$ varies from 3 to 7).

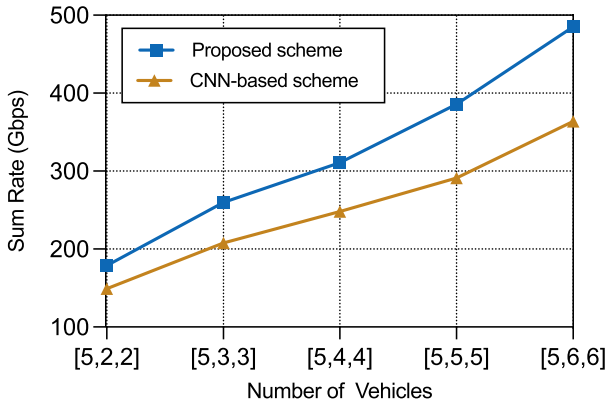

Fig. 13. The sum rate as the number of target vehicles varies ($|\mathcal{K}| = 5$, $|\mathcal{M}|$ and $|\mathcal{N}|$ vary from 2 to 6).

achieve up to 4.05% gain in terms of classification accuracy compared to baseline b. This is due to the fact that the proposed scheme uses separate weight matrices for each type of vehicle, hence, the graph information vectors of different types of vehicles can be better represented.

In Fig. 11, we show how the training loss changes as the number of training iterations varies. From Fig. 11, we see that, as the number of training iterations increases, the training loss of all considered learning algorithms decreases first and, then remains unchanged. The fact that the training loss remains unchanged demonstrates the convergence of the GNN-based

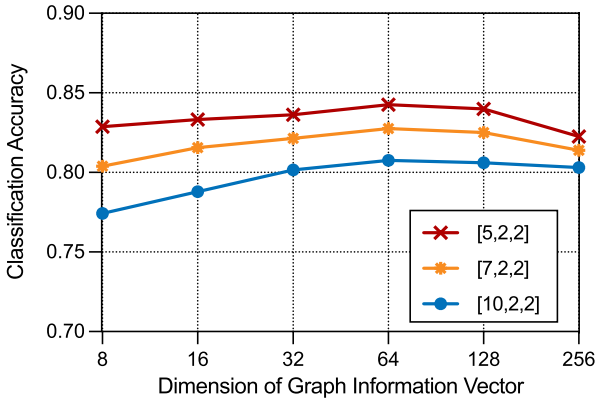

Fig. 14. Impact of the graph information vector dimension λ_0.

algorithm. From Fig. 11, we can also see that the proposed scheme can reduce training loss by 43.17%, compared to baseline b. This is due to the fact that the proposed scheme uses different weight matrices (e.g., $\boldsymbol{w}_2$, $\boldsymbol{w}_3$ and $\boldsymbol{w}_4$) for different type of vehicles, and hence, better graph information vectors can be learned.

In Fig. 12, we show how the sum of data rates of all communication target vehicles changes as the number of communication target vehicles varies. From this figure, we see that, as the number of communication target vehicles increases, the gap between the proposed scheme and baseline b increases. In particular, the proposed algorithm can improve the sum rate of all communication target vehicles by up to 7.75% compared to baseline b when the number of SPVs, communication target vehicles, and sensing target vehicles in the network are $|\mathcal{K}| = 7$, $|\mathcal{M}| = 7$, and $|\mathcal{N}| = 2$, respectively. This is because the vehicle topology is more complicated as the number of communication target vehicles increases. Therefore, homogeneous GNN-based algorithms may not be able to fully extract the graph information from complex vehicle topologies. Compared to a homogeneous GNN-based algorithm, the proposed heterogeneous GNN-based algorithm can extract more vehicle topology features since it uses different weight matrices to represent the features of different type of vehicles.

Fig. 13 shows how the sum of data rates of all communication target vehicles changes as the number of communication and sensing target vehicles varies. Fig. 13 shows that the proposed scheme can achieve up to 19.76% gains in terms of the sum rate of all communication target vehicles compared to the CNN-based method. This is because the proposed scheme can capture the graph information related to vehicle connection, communication interference, and sensing interference of each vehicle.

Fig. 14 shows how the classification accuracy changes as the dimension of graph information vector varies. From Fig. 14, we can see that, as the dimension of graph information vector increases, the classification accuracy increases since better heterogeneous graph representation can be learned. However, as the dimension of graph information vector continues to increase, the performance of all considered algorithms are stabilized. For example, in Fig. 14, all considered algorithms reach the best performance when the dimension of graph

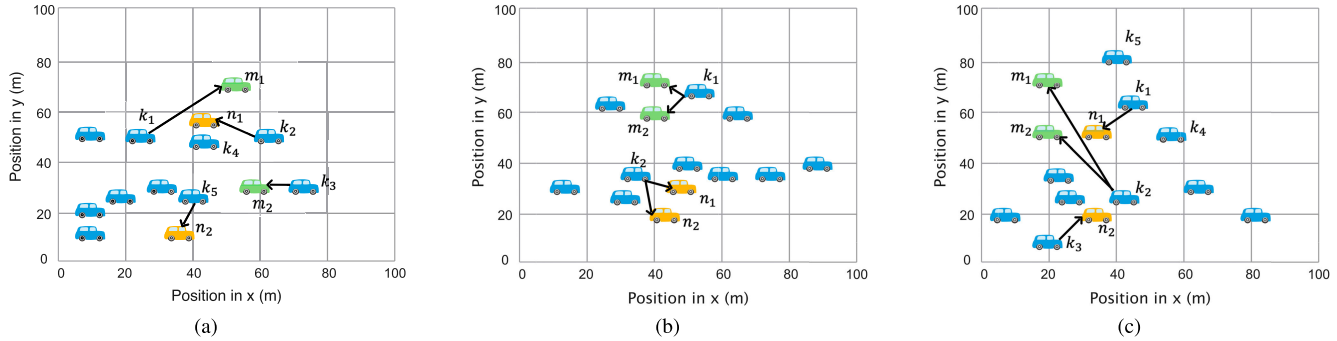

Fig. 15. Visualization of service mode selection and target vehicle association strategy obtained by the proposed method.

information vector λ_0 is 64, and then the performance becomes stable or even slightly worse. This is due to the fact that, the trained GNN model will be over fitted when the dimension of graph information vector becomes too large.

Fig. 15 is a visualization of using our proposed method for determining the mode of service provider vehicles and target vehicle association. In this figure, the blue, yellow, and green points refer to SPVs, sensing target vehicles, and communication target vehicles, respectively. From Fig. 15(a), we can see that the target vehicles do not necessarily select the geographically closest SPV. For example, in Fig. 15(a), sensing target vehicle n_1 selects SPV k_2 instead of its geographically closest SPV k_4. This is because the sensing link between vehicle k_4 and vehicle n_1 will cause interference to the communication link between vehicle k_1 and vehicle m_1. From Fig. 15(b), we can also see that if the geographical locations of two target vehicles are close to each other, an SPV is more likely to provide services for both of them simultaneously. For example, SPV k_1 provides communication services to communication target vehicles m_1 and m_2 at the same time. Fig. 15(c) shows that a sensing target vehicle prefers to select an SPV which can provide a sensing link that is orthogonal to communication links. For example, sensing target vehicle n_1 selects SPV k_1 instead of SPVs k_4, k_5. This is because the directions of the communication link $k_2 \rightarrow m_1$ and the sensing link $k_1 \rightarrow n_1$ are nearly orthogonal and hence, the interference between communication link $k_2 \rightarrow m_1$ and sensing link $k_1 \rightarrow n_1$ can be minimized.

V. Conclusion

In this paper, we developed a novel framework that uses THz for joint communication and sensing in vehicular networks. Our goal was to maximize the sum of data rates of all communication target vehicles while satisfying the sensing service requirements of all sensing target vehicles. To this end, we formulated an optimization problem that jointly considers service mode selection, target vehicle association, THz channel features, and dynamic vehicle topologies. To solve this problem, we developed a novel heterogeneous GNN-based scheme, which can effectively find the strategy of service mode selection and target vehicle association. The proposed scheme enables the trained GNN to quickly adapt to dynamic vehicle topologies with various vehicle types. Simulation results showed that, compared with the baseline methods, the proposed method can achieve significant gains in terms of the sum rate of all communication target vehicles.

References

[1] X. Li, M. Chen, Z. Zhang, D. Liu, Y. Liu, and S. Mao, "Joint optimization of sensing and communications in vehicular networks: A graph neural network-based approach," in *Proc. IEEE Int. Conf. Commun. (ICC)*, Rome, Italy, May 2023, pp. 5781–5786.

[2] M. H. C. Garcia et al., "A tutorial on 5G NR V2X communications," *IEEE Commun. Surveys Tuts.*, vol. 23, no. 3, pp. 1972–2026, 3rd Quart., 2021.

[3] J. A. Zhang et al., "Enabling joint communication and radar sensing in mobile networks—A survey," *IEEE Commun. Surveys Tuts.*, vol. 24, no. 1, pp. 306–345, 1st Quart., 2022.

[4] L. Zhao, D. Wu, L. Zhou, and Y. Qian, "Radio resource allocation for integrated sensing, communication, and computation networks," *IEEE Trans. Wireless Commun.*, vol. 21, no. 10, pp. 8675–8687, Oct. 2022.

[5] C. Chaccour, M. N. Soorki, W. Saad, M. Bennis, P. Popovski, and M. Debbah, "Seven defining features of terahertz (THz) wireless systems: A fellowship of communication and sensing," *IEEE Commun. Surveys Tuts.*, vol. 24, no. 2, pp. 967–993, 2nd Quart., 2022.

[6] X. Chen et al., "Multi-tenant cross-slice resource orchestration: A deep reinforcement learning approach," *IEEE J. Sel. Areas Commun.*, vol. 37, no. 10, pp. 2377–2392, Oct. 2019.

[7] W. Wu et al., "Dynamic RAN slicing for service-oriented vehicular networks via constrained learning," *IEEE J. Sel. Areas Commun.*, vol. 39, no. 7, pp. 2076–2089, Jul. 2021.

[8] M. Shojafar, N. Cordeschi, and E. Baccarelli, "Energy-efficient adaptive resource management for real-time vehicular cloud services," *IEEE Trans. Cloud Comput.*, vol. 7, no. 1, pp. 196–209, Jan. 2019.

[9] N. Cordeschi, D. Amendola, and E. Baccarelli, "Reliable adaptive resource management for cognitive cloud vehicular networks," *IEEE Trans. Veh. Technol.*, vol. 64, no. 6, pp. 2528–2537, Jun. 2015.

[10] A. Liu et al., "A survey on fundamental limits of integrated sensing and communication," *IEEE Commun. Surveys Tuts.*, vol. 24, no. 2, pp. 994–1034, 2nd Quart., 2022.

[11] Y. Zhong et al., "Empowering the V2X network by integrated sensing and communications: Background, design, advances, and opportunities," *IEEE Netw.*, vol. 36, no. 4, pp. 54–60, Jul. 2022.

[12] V. Petrov et al., "On unified vehicular communications and radar sensing in millimeter-wave and low terahertz bands," *IEEE Wireless Commun.*, vol. 26, no. 3, pp. 146–153, Jun. 2019.

[13] X. Mu, Y. Liu, L. Guo, J. Lin, and L. Hanzo, "NOMA-aided joint radar and multicast-unicast communication systems," *IEEE J. Sel. Areas Commun.*, vol. 40, no. 6, pp. 1978–1992, Jun. 2022.

[14] F. Liu, C. Masouros, A. P. Petropulu, H. Griffiths, and L. Hanzo, "Joint radar and communication design: Applications, state-of-the-art, and the road ahead," *IEEE Trans. Commun.*, vol. 68, no. 6, pp. 3834–3862, Jun. 2020.

[15] J. A. Zhang et al., "An overview of signal processing techniques for joint communication and radar sensing," *IEEE J. Sel. Topics Signal Process.*, vol. 15, no. 6, pp. 1295–1315, Nov. 2021.

[16] N. Q. Hieu, D. T. Hoang, N. C. Luong, and D. Niyato, "iRDRC: An intelligent real-time dual-functional radar-communication system for automotive vehicles," *IEEE Wireless Commun. Lett.*, vol. 9, no. 12, pp. 2140–2143, Dec. 2020.

[17] Q. Zhang, X. Wang, Z. Li, and Z. Wei, "Design and performance evaluation of joint sensing and communication integrated system for 5G mmWave enabled CAVs," *IEEE J. Sel. Topics Signal Process.*, vol. 15, no. 6, pp. 1500–1514, Nov. 2021.

[18] Z. Chen et al., "Terahertz wireless communications for 2030 and beyond: A cutting-edge frontier," *IEEE Commun. Mag.*, vol. 59, no. 11, pp. 66–72, Nov. 2021.

[19] A. A. Boulogeorgos, S. K. Goudos, and A. Alexiou, "Users association in ultra dense THz networks," in *Proc. IEEE 19th Int. Workshop Signal Process. Adv. Wireless Commun. (SPAWC)*, Kalamata, Greece, Jun. 2018, pp. 1–5.

[20] B. Chang, X. Yan, L. Zhang, Z. Chen, L. Li, and M. A. Imran, "Joint communication and control for mmWave/THz beam alignment in V2X networks," *IEEE Internet Things J.*, vol. 9, no. 13, pp. 11203–11213, Jul. 2022.

[21] E. Sopin, D. Moltchanov, A. Daraseliya, Y. Koucheryavy, and Y. Gaidamaka, "User association and multi-connectivity strategies in joint terahertz and millimeter wave 6G systems," *IEEE Trans. Veh. Technol.*, vol. 71, no. 12, pp. 12765–12781, Dec. 2022.

[22] L. Xu et al., "Joint location, bandwidth and power optimization for THz-enabled UAV communications," *IEEE Commun. Lett.*, vol. 25, no. 6, pp. 1984–1988, Jun. 2021.

[23] Y. Wu, J. Kokkoniemi, C. Han, and M. Juntti, "Interference and coverage analysis for terahertz networks with indoor blockage effects and line-of-sight access point association," *IEEE Trans. Wireless Commun.*, vol. 20, no. 3, pp. 1472–1486, Mar. 2021.

[24] A. Shafie, N. Yang, S. Durrani, X. Zhou, C. Han, and M. Juntti, "Coverage analysis for 3D terahertz communication systems," *IEEE J. Sel. Areas Commun.*, vol. 39, no. 6, pp. 1817–1832, Jun. 2021.

[25] M. T. Hossan and H. Tabassum, "Mobility-aware performance in hybrid RF and terahertz wireless networks," *IEEE Trans. Commun.*, vol. 70, no. 2, pp. 1376–1390, Feb. 2022.

[26] Z. Sheng, Y. Xu, S. Xue, and D. Li, "Graph-based spatial–temporal convolutional network for vehicle trajectory prediction in autonomous driving," *IEEE Trans. Intell. Transp. Syst.*, vol. 23, no. 10, pp. 17654–17665, Oct. 2022.

[27] Z. Zhao, G. Verma, C. Rao, A. Swami, and S. Segarra, "Distributed scheduling using graph neural networks," in *Proc. IEEE Int. Conf. Acoust., Speech Signal Process. (ICASSP)*, Toronto, ON, Canada, Jun. 2021, pp. 4720–4724.

[28] H. Qiu, Q. Zheng, M. Msahli, G. Memmi, M. Qiu, and J. Lu, "Topological graph convolutional network-based urban traffic flow and density prediction," *IEEE Trans. Intell. Transp. Syst.*, vol. 22, no. 7, pp. 4560–4569, Jul. 2021.

[29] Y. Su et al., "Trajectory forecasting based on prior-aware directed graph convolutional neural network," *IEEE Trans. Intell. Transp. Syst.*, vol. 23, no. 9, pp. 16773–16785, Sep. 2022.

[30] Z. He, L. Wang, H. Ye, G. Y. Li, and B. F. Juang, "Resource allocation based on graph neural networks in vehicular communications," in *Proc. IEEE Global Commun. Conf.*, Dec. 2020, pp. 1–5.

[31] K. Hou, Q. Xu, X. Zhang, Y. Huang, and L. Yang, "User association and power allocation based on unsupervised graph model in ultra-dense network," in *Proc. IEEE Wireless Commun. Netw. Conf. (WCNC)*, Nanjing, China, Mar. 2021, pp. 1–6.

[32] M. Lee, G. Yu, and G. Y. Li, "Graph embedding-based wireless link scheduling with few training samples," *IEEE Trans. Wireless Commun.*, vol. 20, no. 4, pp. 2282–2294, Apr. 2021.

[33] Y. Shen, Y. Shi, J. Zhang, and K. B. Letaief, "Graph neural networks for scalable radio resource management: Architecture design and theoretical analysis," *IEEE J. Sel. Areas Commun.*, vol. 39, no. 1, pp. 101–115, Jan. 2021.

[34] Gurobi. *Gurobi Optimization*. Accessed: 2021. [Online]. Available: https://www.gurobi.com

[35] A. Fox, B. V. K. V. Kumar, J. Chen, and F. Bai, "Multi-lane pothole detection from crowdsourced undersampled vehicle sensor data," *IEEE Trans. Mobile Comput.*, vol. 16, no. 12, pp. 3417–3430, Dec. 2017.

[36] M. Chen et al., "Distributed learning in wireless networks: Recent progress and future challenges," *IEEE J. Sel. Areas Commun.*, vol. 39, no. 12, pp. 3579–3605, Dec. 2021.

[37] M. Chen, Z. Yang, W. Saad, C. Yin, H. V. Poor, and S. Cui, "A joint learning and communications framework for federated learning over wireless networks," *IEEE Trans. Wireless Commun.*, vol. 20, no. 1, pp. 269–283, Jan. 2021.

[38] L. Ma, N. Cheng, X. Wang, R. Sun, and N. Lu, "On-demand resource management for 6G wireless networks using knowledge-assisted dynamic neural networks," in *Proc. IEEE Int. Conf. Commun.*, Seoul, South Korea, May 2022, pp. 1–6.

[39] X. Wang et al., "Joint flying relay location and routing optimization for 6G UAV-IoT networks: A graph neural network-based approachs," *Remote Sens.*, vol. 14, no. 17, pp. 1–26, Sep. 2022.

[40] P. Veličković, G. Cucurull, A. Casanova, A. Romero, P. Liò, and Y. Bengio, "Graph attention networks," in *Proc. Int. Conf. Learn. Represent. (ICLR)*, Vancouver, BC, Canada, Feb. 2018, pp. 1–12.

[41] W. L. Hamilton, R. Ying, and J. Leskovec, "Inductive representation learning on large graphs," in *Proc. Conf. Neural Inf. Process. Syst. (NIPS)*, Long Beach, CA, USA, Dec. 2017, pp. 1–19.

[42] CSIRO. (2018). *Stellargraph Machine Learning Library*. [Online]. Available: https://github.com/stellargraph/stellargraph

[43] X. Huang, S. Zeng, D. Li, P. Zhang, S. Yan, and X. Wang, "Fair computation efficiency scheduling in NOMA-aided mobile edge computing," *IEEE Wireless Commun. Lett.*, vol. 9, no. 11, pp. 1812–1816, Nov. 2020.

[44] K. He and J. Sun, "Convolutional neural networks at constrained time cost," in *Proc. IEEE Conf. Comput. Vis. Pattern Recognit. (CVPR)*, Boston, MA, USA, Jun. 2015, pp. 5353–5360.

[45] D. Zhao, Y. Gao, Z. Zhang, Y. Zhang, and T. Luo, "Prediction of vehicle motion based on Markov model," in *Proc. Int. Conf. Comput. Syst., Electron. Control (ICCSEC)*, Dalian, China, Dec. 2017, pp. 205–209.

Xuefei Li (Graduate Student Member, IEEE) received the B.E. degree from the Beijing University of Posts and Telecommunications, Beijing, China, where she is currently pursuing the Ph.D. degree with the School of Information and Communication Engineering. Her research interests include wireless communications, vehicular networks, and machine learning.

Mingzhe Chen (Member, IEEE) is currently an Assistant Professor with the Department of Electrical and Computer Engineering and the Institute of Data Science and Computing, University of Miami. His research interests include federated learning, reinforcement learning, virtual reality, unmanned aerial vehicles, and the Internet of Things. He received four journal paper awards from the IEEE Communication Society, including the Young Author Best Paper Award in 2021 and 2023, the Fred W. Ellersick Prize Award in 2022, and the IEEE Marconi Prize Paper Award in Wireless Communications in 2023, and four conference best paper awards from IEEE ICC in 2020, IEEE GLOBECOM in 2020, IEEE WCNC in 2021, and ICCCN in 2023. He serves as an Associate Editor for IEEE TRANSACTIONS ON MOBILE COMPUTING, IEEE WIRELESS COMMUNICATIONS LETTERS, IEEE TRANSACTIONS ON GREEN COMMUNICATIONS AND NETWORKING, and IEEE TRANSACTIONS ON MACHINE LEARNING IN COMMUNICATIONS AND NETWORKING.

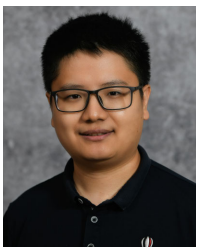

Yuchen Liu (Member, IEEE) received the Ph.D. degree from the Georgia Institute of Technology, USA. He is currently an Assistant Professor with the Department of Computer Science, North Carolina State University, USA. His research interests include wireless networking, generative AI, reinforcement learning, mobile computing, and software simulation. He received several best paper awards from IEEE and ACM conferences. He serves as an Associate Editor for IEEE TRANSACTIONS ON GREEN COMMUNICATIONS AND NETWORKING and *International Journal of Sensors, Wireless Communications and Control*.

Zhilong Zhang (Member, IEEE) received the B.E. degree in communication engineering from the University of Science and Technology, Beijing, China, in 2007, and the M.S. and Ph.D. degrees in communication and information systems from the Beijing University of Posts and Telecommunications (BUPT), Beijing, in 2010 and 2016, respectively. From 2010 to 2012, he was a Software Engineer with TD Tech Ltd., Beijing. From 2014 to 2015, he was a Visiting Scholar with Stony Brook University, Stony Brook, NY, USA. He is currently an Associated Professor with BUPT. His research interests include optimization theory and its applications in wireless video transmissions and wireless networks.

Danpu Liu (Senior Member, IEEE) received the Ph.D. degree in communication and electrical systems from the Beijing University of Posts and Telecommunications, Beijing, China, in 1998. She was a Visiting Scholar with the City University of Hong Kong in 2002, The University of Manchester in 2005, and the Georgia Institute of Technology in 2014. She is currently with the Beijing Key Laboratory of Network System Architecture and Convergence, Beijing University of Posts and Telecommunications. Her current research interests include B5G/6G mobile communications and air-space-ground integrated networks.

Shiwen Mao (Fellow, IEEE) received the Ph.D. degree in electrical and computer engineering from Polytechnic University, Brooklyn, NY, USA. He is currently a Professor, an Earle C. Williams Eminent Scholar, and the Director of the Wireless Engineering Research and Education Center, Auburn University. His research interests include wireless networks and multimedia communications. He was a co-recipient of the 2004 IEEE Communications Society Leonard G. Abraham Prize in the Field of Communications Systems, the IEEE Vehicular Technology Society 2020 Jack Neubauer Memorial Award, the 2021 Best Paper Award of Elsevier/KeAi Digital Communications and Networks, the 2021 IEEE INTERNET OF THINGS JOURNAL Best Paper Award, the 2021 IEEE Communications Society Outstanding Paper Award, and several best IEEE ComSoc Technical Committee and conference paper/demo awards. He is a Distinguished Lecturer of the IEEE Communications Society and the IEEE Council of RFID. He is the Editor-in-Chief of IEEE TRANSACTIONS ON COGNITIVE COMMUNICATIONS AND NETWORKING.